Talanta 280 (2024) 126535

Contents lists available at ScienceDirect

Talanta

journal homepage: www.elsevier.com/locate/talanta

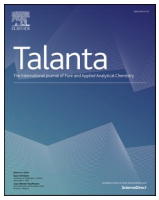

Interfacial modification of recombinant protein for immunoglobulin G adsorption with spindle-shaped MOF as nano molecular containers

Kai Wang [a,1], Hongjin Zhang [c,1], Nishan Jin [a], Yutian Zhou [c], Xinli Guo [c], Wenbin Zhong [c], Xin Li [b], Xuwen Li [d,**], Yang Zhang [a,*]

[a] Shenyang Key Laboratory of Medical Molecular Theranostic Probes in School of Pharmacy, Shenyang Medical College, 146 Huanghe North Avenue, Shenyang, 110034, China
[b] Department of Science and Technology, Shenyang Medical College, 146 Huanghe North Avenue, Shenyang, 110034, China
[c] School of Basic Medicine, Shenyang Medical College, 146 Huanghe North Avenue, Shenyang, 110034, China
[d] Department of Analytical Chemistry, College of Chemistry, Jilin University, Changchun, 130012, China

ARTICLE INFO

Handling editor: Prof. J. Wang

Keywords:
Metal-organic framework
Immunoglobulin G
Protein separation
Purification

ABSTRACT

Development of fresh solid phase extractant is critical for selective separation and purification of special proteins. Herein, we demonstrated a recombinant Staphylococcal Protein G (rSPG) with a His-tag modified the novel single-metal organic framework (rSPG@Ni-MOF-74). The proposed solid-phase extraction material possessed a uniform spindle-shaped structure, large surface area (709.60 $m^2 g^{-1}$) and pore volume (0.08 $m^3 g^{-1}$), high metal content (22.57 wt%), which facilitated the interaction between host and guest. As results, the composite displayed outstanding selective recognition and adsorption of IgG, due to synergistic effect of the binding ability of rSPG with the Fc region of IgG, maintained through hydrogen bonding and electrostatic attraction, as well as hydrophobic interaction. The adsorption performance and mechanism of rSPG@Ni-MOF-74 have been fully investigated. Additionally, the rSPG@Ni-MOF-74 composite could effectively separate IgG from serum obtained from healthy humans, with the purity of the separated IgG verified through SDS-PAGE analysis. Furthermore, LC-MS/MS analysis identified a high content of IgG (55.3 %) in the eluate from rSPG@Ni-MOF-74, suggesting the great potential of rSPG@Ni-MOF-74 in IgG separation and enrichment from complex matrix.

1. Introduction

Immunoglobulin is an antibody-like substance produced by lymphocytes in vertebrates as part of the immune response to antigen stimulation. It is capable of binding directly to the specific antigen and carries out multiple biological functions, thereby significantly boosting immunity and defending against bacterial and viral infections. There are five main types of immunoglobulins: IgA, IgD, IgE, IgG, and IgM [1]. Among them, IgG is the main antibody type in human blood and extracellular fluid, accounting for 70–75 % of total immunoglobulins [2]. As previous reported, a strong correlation has been discovered between IgG antibodies and the triggering of neurotoxicity by IgG aggregates, which supports the use of IgG as a biomarker in plasma for multiple sclerosis [3]. IgG extracted from serum can also serve as a therapeutic drug, as seen in intravenous immunoglobulin therapy (IVIG) used for treating immune deficiency disorders and specific autoimmune conditions [4]. Clinical studies have shown that intravenous administration of immunoglobulin has certain efficacy in treating Kawasaki disease [5]. In addition, extracted IgG from serum can be used to produce biopharmaceuticals such as antibody drugs, vaccines, and diagnostic kits. These biopharmaceuticals have important applications and commercial value in medical and life sciences. Currently, commonly used methods for isolating/extracting IgG include affinity chromatography [6], size exclusion chromatography [7], and liquid chromatography [8]. However, these methods have various drawbacks, such as non-specific binding occurs in affinity chromatography [9], size exclusion chromatography is costly [10], and liquid chromatography has the disadvantages of relatively high cost, long processing time, and complex operation [11]. In recent years, solid-phase extraction methods using nanomaterials as adsorbents have received increasing attention for IgG

* Corresponding author.
** Corresponding author.
E-mail addresses: lixw@jlu.edu.cn (X. Li), zhangyangpro@symc.edu.cn (Y. Zhang).
[1] These authors contributed equally to this work.

https://doi.org/10.1016/j.talanta.2024.126535
Received 20 May 2024; Received in revised form 24 June 2024; Accepted 8 July 2024
Available online 9 July 2024

separation. Compared with traditional precipitation or column chromatography, solid-phase extraction methods using nanomaterials as adsorbents have advantages, such as low cost, simplicity, and reusability. Currently, commonly used solid-phase extraction materials include magnetic nanoparticles, carbon-based nanomaterials, sulfide nanomaterials, and metal-organic frameworks (MOFs). Magalhães FF et al. [12] successfully recovered IgG from rabbit serum by employing magnetic iron oxide nanoparticles (Fe_3O_4, magnetite) coated with hybrid shells composed of a siliceous material modified with the anionic polysaccharide κ-carrageenan. Wang et al. [13] prepared boronic acid derivative-modified molybdenum disulfide nanosheets, achieving specific separation and enrichment of IgG.

MOFs also known as porous coordination polymers (PCPs), exhibiting significant features such as high surface area, tunable pore structures, easy synthesis, and excellent biocompatibility, which make them promising in sample preparation applications [14]. Chen et al. [15] synthesized a magnetic material called mMOF-FBP by attaching Zr-based metal-organic frameworks (Zr-MOFs) to the surface of magnetic microspheres. The abundance of amino groups within Zr-MOFs and hydroxyl groups within FBP molecules confers excellent hydrophobic properties to the material, resulting in high adsorption efficiency for immunoglobulin G (IgG). However, in certain environments, the interaction between metal ions and organic ligands within MOFs might weaken, potentially resulting in decreased stability [16]. Additionally, MOFs suffer from non-specific adsorption during sample pretreatment, limiting their applicability in practical sample analysis. To enhance stability and selectivity, various strategies have been developed, with MOFs modification being the most common. For instance, Wang et al. [17] found that UiO-66-NH_2, a Zr-based MOF, exhibited good adsorption capacity for phosphorylated proteins but displayed significant non-specific adsorption towards other proteins. To address this issue, researchers modified UiO-66-NH_2 with imidazolium-based ionic liquids (ILs) to reduce non-specific adsorption of non-phosphorylated proteins. The modified UiO@IL material exhibited strong hydrophilicity on its surface, significantly reducing hydrophobic and electrostatic interactions between the adsorbent and non-phosphorylated proteins. Concurrently, the imidazole group in ILs interacting with the phosphate group in phosphorylated proteins ensured the excellent adsorption capabilities of UiO@IL towards phosphoproteins. Staphylococcal protein G (SPG) is a protein that can be found in the cell wall of G and C type streptococci [18]. It specifically binds to the Fc region of IgG molecules without affecting their ability to bind antigen via the Fab region. Natural SPG contains binding domains for IgG, as well as domains for albumin and cell surface binding. Recombinant SPG is produced by removing the albumin and cell wall binding domains, while retaining the IgG binding domain, thereby significantly enhancing its specificity. rSPG is a protein composed of amino acids, and its amino acid sequence is synthesized using genetic engineering techniques or obtained through transgenic expression. The amino acids are connected in a particular sequence to create the sequence of amino acids of recombinant SPG, dictating the protein's structure and function in three dimensions. Moreover, the thermal and chemical stability of rSPG ensures that its structure and function are not constrained by experimental conditions [19].

In this study, a single-metal organic framework (Ni-MOF-74) was constructed, which possesses strong stability and a high surface area, making it suitable as an adsorbent for IgG. We modified rSPG onto the surface of Ni-MOF-74 through coordination bonds and hydrogen bonding interactions, resulting in a novel solid-phase extraction material (rSPG@Ni-MOF-74). Due to the high surface area of Ni-MOF-74 and the high selectivity of rSPG towards IgG, as well as the synergy of other forces, resulting in the excellent adsorption capability of rSPG@Ni-MOF-74. Additionally, we successfully selectively extracted and purified IgG from healthy human serum by the proposed adsorbent.

2. Experimental section

2.1. Materials and reagent

Nickel (II) nitrate ($Ni(NO_3)_2$) and hexadecyltrimethylammonium bromide (CTAB) were purchased from Sinopharm Chemical Reagent Co. Ltd. (China). N, N-dimethylformamide (DMF), ethanol was analytical grade (AR) and obtained from Energy Chemical Company. Human serum albumin (HSA), sodium dodecyl sulfate (SDS), Glycine (Gly), and Tris(hydroxymethyl)aminomethane (Tris) were purchased from Biosharp Co., Ltd. Bovine immunoglobulin G (IgG) and transferrin (Trf) were obtained from Shanghai Yuan Ye Biotechnology Co., Ltd. and Sigma-Aldrich Company, respectively. Potassium Chloride (KCl), N,N′-Methylenediacrylamide, ammonium persulfate (APS), Coomassie Brilliant Blue G-250, and Coomassie Brilliant Blue R-250 were purchased from Shanghai National Pharmaceutical Reagent Co., Ltd. The protein molecular weight marker used in the experiment (Broad, 3597A, Takara Biotechnology Co, LTD, Dalian, China) is a mixture of eight purified proteins (myosphere protein, Mw 200 kDa; β-galactosidase, Mw 116 kDa; Phosphorylase b, Mw 97.2 kDa; Serum albumin, Mw 66.4 kDa; Ovalbumin, Mw 44.3 kDa; Carbonic anhydrase, Mw 29.0 kDa; Trypsin inhibitor, Mw 20.1 kDa; Lysozyme, Mw 14.3 kDa). The aforementioned reagents all are the analytical grade and used without further processing. All experiments were conducted using deionized water with a resistivity of 18 MΩ cm.

2.2. Instrumentation

Scanning Electron Microscopy (SEM, Hitachi, HORIBA EMAX mics2) was used to observe the particle size and morphology. Fourier Transform Infrared (FT-IR) spectra were obtained by using a Nicolet 6700 spectrometer from Thermo Electron Corporation. X-ray Diffraction (XRD) patterns were measured on a D8 advance 2500 (Bruker) diffractometer, with XRD intensity data collected in the range of 2θ from 5° to 80° at room temperature. X-ray Photoelectron Spectroscopy (XPS) scan curves were obtained using a Thermo Escalab 250XI instrument. The specific surface area (BET) was conducted on a Micromeritics ASAP2460 instrument from the United States. Thermogravimetric analysis (TGA) was performed on a TGA/DSC 3+ analyzer (Mettler Toledo Company, Switzerland) at a heating rate of 10 °C min^{-1} under nitrogen atmosphere. LC-MS/MS analysis was carried out on an Easy nano-LC 1000 system (Thermo Fisher Scientific, Germany) interfaced with a Q Exactive Orbitrap mass spectrometer (Thermo Fisher Scientific, Germany). T6 UV–Vis spectrophotometer (Beijing Puxi General Instrument Co. Ltd., China) was used in protein quantification. The circular dichroism (CD) spectra were recorded with a MOS-450 spectrometer/polarimeter (Biologic Science Instrument, France).

2.3. Synthesis of rSPG@Ni-MOF-74

1.0 g of $Ni(NO_3)_2$, 0.39 g of 2,5-dihydroxyterephthalic acid and 0.1 g of CTAB were added into mixed solution containing 75 mL of DMF, 5 mL of ethanol, and 5 mL of water stirred for 20 min, following added 100 μL glacial acetic acid under the stirring state. Label this mixture as the standard solution. Subsequently, transferred the standard solution into a stainless steel autoclave at 120 °C for 24 h. After the reaction was complete, washed the obtained production three times with DMF, and then centrifuged at 10000 rpm. Finally, the production experienced vacuum drying at 80 °C to obtain Ni-MOF-74. Following, 50 mg of rSPG was dissolved in 10 mL H_2O to prepare a concentrated stock solution of 5 mg mL^{-1}. Take 200 μL of the rSPG stock solution and add 3.8 mL of H_2O to dilute it to a final concentration of 250 μg mL^{-1} 6 mg of Ni-MOF-74 was added it into the protein solution and kept shocking vigorously for 3 h, the mixture was centrifuged at 6000 rpm for 10 min and washed twice with H_2O, and final production was subjected to freeze-drying and stored for future used.

2.4. Selective adsorption of IgG

To investigate the selective adsorption property of the as-prepared rSPG@Ni-MOF-74, three proteins with distinct structures, hydrodynamic size and isoelectric point (pI), i.e., human serum albumin (HSA, MW 66 kD, pI 5.4), immunoglobulin G (IgG, MW 150 kDa. pI 8.0), and transferrin (Trf, MW 450 kDa, pI 5.4) were utilized as representative model guest molecules to study the adsorption characteristics of rSPG@Ni-MOF-74. Proteins with identical concentrations were subjected to adsorption experiments at different pH levels. The pH of the solution was adjusted using a 40 mmol L^{-1} Britton-Robinson (BR) buffer spanning from pH 4 to 11.

1.0 mg of rSPG@Ni-MOF-74 was added into 2 mL of standard protein sample solutions with a concentration of 100 μg mL^{-1}. The mixture was agitated for 30 min under ambient conditions to aid in the adsorption process, and then the solution was centrifuged at 6000 rpm for 5 min. The supernatant was collected to measure residual proteins by quantifying the soret absorbance at 590 nm using a UV–visible spectrophotometer after staining with Coomassie brilliant blue for HSA, Trf, and IgG. The efficiency of IgG adsorption on the rSPG@Ni-MOF-74 (denoted as E_1) was calculated using formula (1):

$$E_1 = \frac{C_0 - C_1}{C_0} \times 100\% \quad (1)$$

In the equation, C_0 represents the initial concentration (μg mL^{-1}) of the IgG solution, and C_1 represents the concentration (μg mL^{-1}) of IgG in the supernatant after extraction.

The adsorption property on the rSPG@Ni-MOF-74 was investigated through adsorption kinetics and thermodynamics. The kinetic behavior of proteins on rSPG@Ni-MOF-74 was studied at room temperature over a time range of 0–60 min. The thermodynamic behavior of IgG on rSPG@Ni-MOF-74 was studied with the protein concentration range of 100–1000 μg mL^{-1}. equation (2) was utilized to calculate the adsorption capacity.

$$Q = \frac{(C_0 - C_e) \times V}{m}$$

$$Q = \frac{(C_0 - C_e) \times m}{V} \quad (2)$$

C_0 and C_e (μg mL^{-1}) represent the initial and final concentrations of IgG in the solution, respectively. V denotes the volume of the protein solution (mL), and m stands for the mass of the rSPG@Ni-MOF-74 (mg).

Equations (3) and (4) described the linear shapes of the pseudo-first-order (PFO) and pseudo-second-order (PSO) models, respectively.

$$\ln(Q_e - Q_t) = \ln Q_e - k_1 t \quad (3)$$

$$\frac{t}{Q_t} = \frac{t}{Q_e} + \frac{1}{k_2 Q_e^2} \quad (4)$$

The adsorption capacity at any given time t (min) is represented by Qt.

(mg g^{-1}), while the equilibrium adsorption capacity of IgG is represented by Q_e

(mg g^{-1}). The equilibrium rate constant of the pseudo first-order sorption is denoted as k_1 (min^{-1}), and the equilibrium rate constant of the pseudo second-order sorption is denoted as k_2 (g mg^{-1} min^{-1}).

Equations (5) and (6) depict the fitting equations of the Langmuir model and Freundlich model, respectively.

$$\frac{C_e}{Q_e} = \frac{1}{Q_m k_L} + \frac{C_e}{Q_m} \quad (5)$$

$$\ln Q_e = \ln k_F + \frac{1}{n} \ln C_e \quad (6)$$

C_e (mg L^{-1}) and Q_e (mg g^{-1}) represent the equilibrium concentration and equilibrium adsorption capacity of IgG, respectively. Q_m (mg g^{-1}) is the theoretical maximum adsorption capacity of IgG adsorbed per unit mass of samples. k_L (L mg^{-1}) is the constant related to the *Langmuir* adsorption, and k_F is the constant related to the *Freundlich* adsorption. The parameter $1/n$ is an empirical factor associated with surface heterogeneity or adsorption intensity.

2.5. Elution of IgG

After the adsorption process, the supernatant was discard, and 0.5 % SDS solution was added and agitated for 30 min to achieve complete elution. Then, the supernatant was taken after centrifuging for 5 min at 6000 rpm, and the absorbance of protein was measured after staining to calculate the elution efficiency. Furthermore, we evaluated the reusability of rSPG@Ni-MOF-74 by performing 5 adsorption/desorption cycles. The elution efficiency (E_2) was calculated using formula (7):

$$E_2 = \frac{C_2}{C_0 - C_1} \times 100\% \quad (7)$$

Where E_2 is the elution efficiency (%) of IgG. C_0 is the initial concentration (μg mL^{-1}) of IgG in the experiment. C_1 is the concentration (μg mL^{-1}) of IgG in the solution after adsorption. C_2 is the concentration (μg mL^{-1}) of IgG in the solution after elution.

2.6. Selective isolation of IgG from human serum

Healthy human serum was diluted 200-fold with a NaCl solution (500 mM, pH 8.0). Take 200 μL of serum and add 0.6 mg rSPG@Ni-MOF-74, following shaken well for 30 min and centrifuged for 5 min at 6000 rpm, and then the serum samples before and after adsorption were collected. Pre-washed the adsorbed proteins on rSPG@Ni-MOF-74 with 0.1 % SDS, and recovered the proteins using 0.5 % SDS as the eluent. Finally, the collected eluents experienced sodium dodecyl sulfate-polyacrylamide gel electrophoresis (SDS-PAGE) and mass analysis.

3. Results and discussion

3.1. Synthesis and characteristics of rSPG@Ni-MOF-74

The synthesis procedure of rSPG@Ni-MOF-74 was depicted in Scheme 1. Ni-MOF-74 formed by the periodic network structure of transition metal ions (Ni^{2+}) and organic ligands. It possessed tunable structure, surface porosity, and coordinatively unsaturated nickel ions. The coordinatively unsaturated nature of Ni-MOF-74 gaveIt adsorption potential, as it could interact with other substances and form new coordination complexes. The rSPG used in this study contains a His-tag, with a singleImidazole group on the histidine residue that could form a metal coordination bond with the coordinatively unsaturated Ni^{2+} ions, thereby binding to the surface of.

Ni-MOF-74 [20]. Fig. 1A-B and S1A-B depicted the SEM images of rSPG@Ni-MOF-74 and Ni-MOF-74. The obtained Ni-MOF-74 have a uniform spindle structureWith an average diameter of approximately 1.0 μm. These single spindle structure aggregated to form a cauliflower-like appearance. After modification of rSPG, we could observe that the spindle structure of single particle and aggregated cauliflower-like appearance were still maintained, suggesting that the modified rSPG hardly have impact the fundamental structure of Ni-MOF-74. However, compared with Ni-MOF-74, the average particle diameter of rSPG@Ni-MOF-74 significantly increased. The XRD pattern of Ni-MOF-74 revealed two major peaks occurring at $2\theta = 6.90°$ and 11.92°, consistent with previous reports (Fig. 1C). The primary peaks of rSPG@Ni-MOF-74 were observed at $2\theta = 6.65°$ and 11.65°, mirroring the positions of Ni-MOF-74 peaks, auxiliary evidence demonstrating the successful synthesis of rSPG@Ni-MOF-74 without altering the basic framework structure of Ni-MOF-74. High metal content (22.57 wt%)

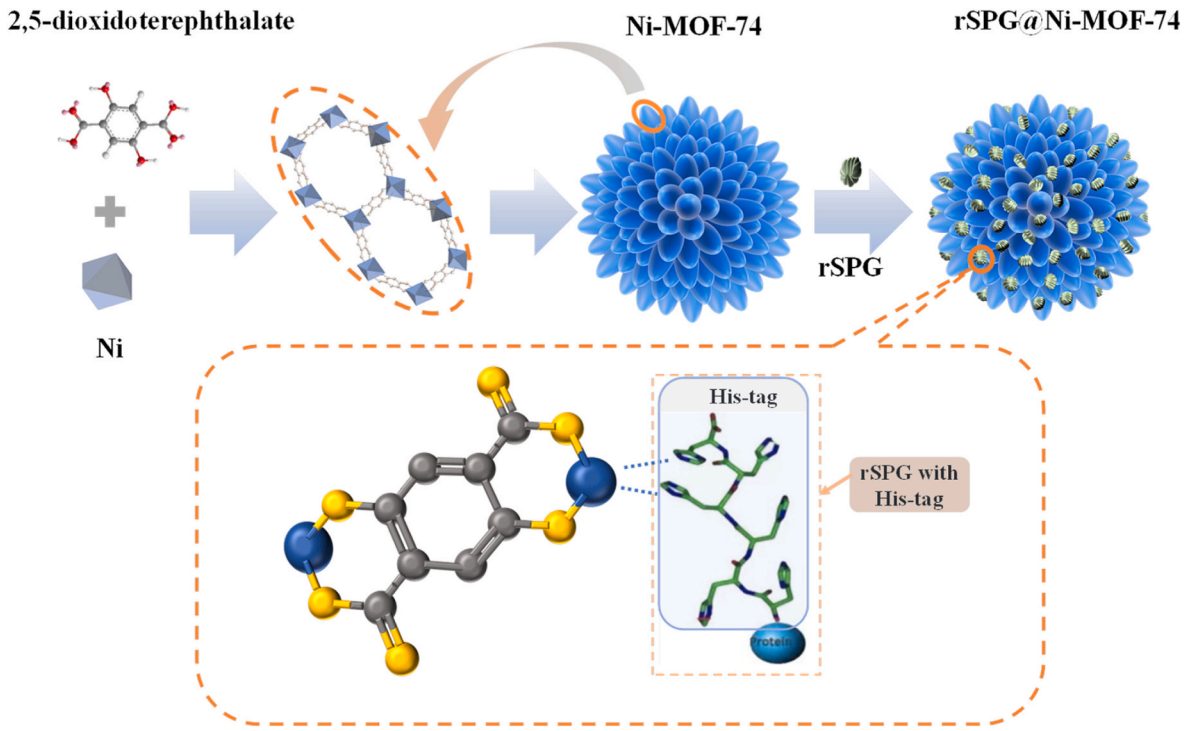

Scheme 1. Synthetic route of rSPG@Ni-MOF-74.

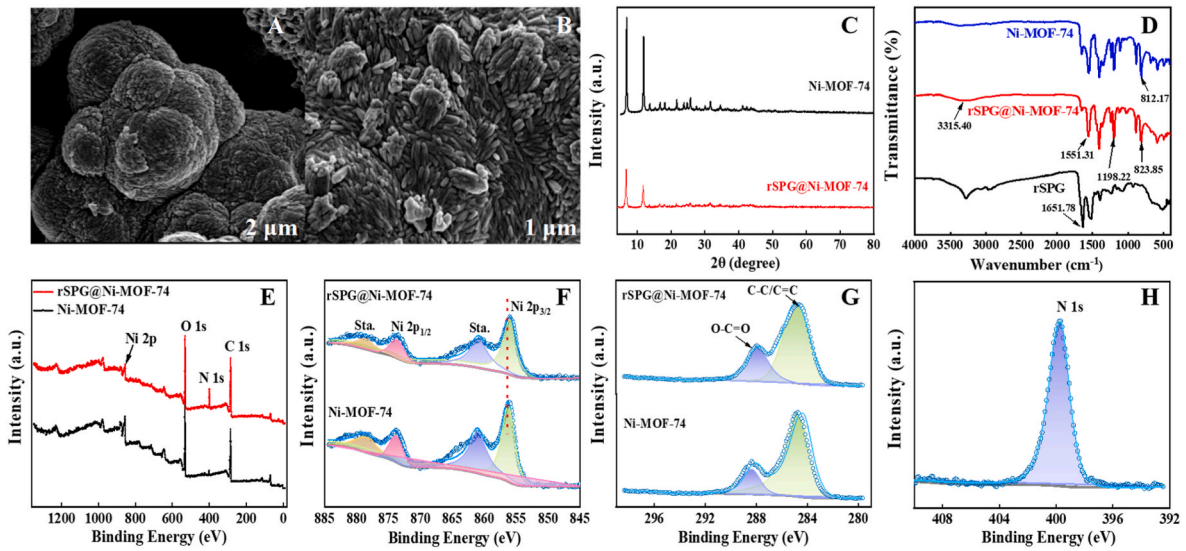

Fig. 1. SEM images of rSPG@Ni-MOF-74 (A B). Raman spectra of Ni-MOF-74 and rSPG@Ni-MOF-74 (C). FT-IR spectra of Ni-MOF-74, rSPG@Ni-MOF-74 and His-rSPG (D). High-resolution Ni 2p (F), C 1s (G), and N 1s (H) XPS spectra of Ni-MOF-74 and rSPG@Ni-MOF-74 (E).

was roughly evaluated by the thermogravimetric analysis (TGA) of rSPG@Ni-MOF-74 (Fig. S2). Fourier-transform infrared (FT-IR) spectra of Ni-MOF-74, rSPG@Ni-MOF-74, and rSPG were shown in Fig. 1D. In Ni-MOF-74, the peaks located at 1551.31 cm^{-1} and 1346.87 cm^{-1} can be attributed to the stretching vibrations of carboxyl groups within the framework of Ni-MOF-74. The peaks at 1196.77 cm^{-1} and 1112.68 cm^{-1} represent the stretching vibrations of C–H single bonds and C═O double bonds in aromatic rings, respectively. The peak at 885.05 cm^{-1} corresponds to the out-of-plane bending vibration of the benzene ring [21, 22]. Additionally, a peak observed at 812.17 cm^{-1} represents the stretching and in-plane bending vibrations caused by the Ni–O bonds [23], which are characteristic chemical bonds of Ni-MOF-74. In the spectrum of the rSPG@Ni-MOF-74 composite material, a new peak appears at 3315.40 cm^{-1} has been observed, which can be explained by the stretching vibrations of O–H and N–H present in rSPG [24]. These peaks matched the vibrations observed in the spectrum of rSPG, suggesting the existence of proteins in rSPG@Ni-MOF-74. The peak corresponding to the stretching and in-plane bending vibrations caused by Ni–O bonds in rSPG@Ni-MOF-74 is shifted to 823.85 cm^{-1} compared to Ni-MOF-74. Due to the imidazole ring contained within the His-tag of rSPG, it could form a metal coordination bond with Ni-MOF-74, indicating successful binding of rSPG to Ni-MOF-74. Additionally, in the spectrum of rSPG, a peak at 1651.78 cm^{-1} corresponded to the vibration of amide I groups in protein molecules, representing the stretching vibration of carbonyl (C═O) bonds. However, in the spectrum analysis of rSPG@Ni-MOF-74, the intensity of this peak was reduced. This

reduction was attributed to the formation of ionic bonds between nickel ions and the carboxyl groups in proteins, which weaken the intensity of this peak and slightly shifts its position. The N_2 adsorption/desorption isotherm showed in Fig. S3 for rSPG@Ni-MOF-74 displays typical type-IV sorption isotherms accompanied by an H_2 hysteresis loop. The presence of irregular pores within rSPG@Ni-MOF-74 was responsible for the hysteresis loop observed within the P/P° range of 0.4–0.9. Table S1 list the specific surface area and total pore volume of Ni-MOF-74 and rSPG@Ni-MOF-74. It was observed that rSPG@Ni-MOF-74 exhibited an increased specific surface area and total pore volume, which could be attributed to the pore expansion or formation of new pores caused by rSPG modification, leading to an increase in the surface area of rSPG@Ni-MOF-74. The XPS survey spectrum of Ni-MOF-74 displayed characteristic peaks corresponding to C 1s (284.70 eV), O 1s (531.74 eV), and Ni 2p (855.90 eV) [25] (Fig. 1E). The XPS survey spectrum of rSPG@Ni-MOF-74 exhibited an additional characteristic peak at N 1s (399.69 eV), which could be attributed to the presence of O═C–N groups [26] in rSPG. Fig. 1F showed the Ni 2p high-resolution XPS spectra of Ni-MOF-74 and rSPG@Ni-MOF-74. The Ni 2p spectrum of Ni-MOF-74 revealed two peaks at 856.23 eV and 861.03 eV for Ni $2p_{3/2}$ and two peaks at 873.90 eV and 879.70 eV for Ni $2p_{1/2}$, suggesting the valence state of Ni is +2. The major spin-orbit peak appeared at 856.23 eV and 873.90 eV, with satellite peaks at 861.03 eV and 879.70 eV [27]. However, in the Ni 2p spectrum of rSPG@Ni-MOF-74, both the major spin-orbit peaks shifted towards lower binding energies at 856.23 eV and 873.60 eV. This shift could be attributed to the formation of metal coordination bonds, which affected the charge transfer between ligands and nickel ions, leading to changes in the electronic energy levels associated with the metal coordination bond [28]. Fig. 1G showed the C 1s high-resolution XPS spectra of Ni-MOF-74 and rSPG@Ni-MOF-74, two characteristic peaks at 284.70 eV and 288.50 eV were corresponded to C–C/C═C and O–C═O, respectively. Fig. 1H represented the N 1s spectrum of rSPG@Ni-MOF-74, which provided by the modified rSPG.

3.2. Protein adsorption behavior of the rSPG@Ni-MOF-74

In general, in the case of protein adsorption onto metal-immobilized adsorbents, the driving forces typically include both specific interactions like affinity binding and non-specific interactions such as electrostatic and hydrophobic interactions. All of these interactions must be considered when evaluated protein adsorption behaviors onto the rSPG@Ni-MOF-74 composite.

In this case, to evaluate the performance of rSPG@Ni-MOF-74 in protein adsorption, three high-abundance proteins HSA (pI 4.7), IgG (pI 8.0) and Trf (pI 5.4) are selected as model proteins. As results, the adsorption process showed the pH-dependent over a wide pH range (Fig. 2A), and the maximum adsorption efficiency was obtained near the isoelectric point (pI) of each protein: pH 4.0 for HSA, pH 8.0 for IgG, and pH 5.0 for Trf (with minimal adsorption for HSA and Trf). As the pH approaches the isoelectric point, the proteins are neutral, exposing hydrophobic residues in their structure, which promoted hydrophobic interactions between the rSPG@Ni-MOF-74 composite and the proteins and facilitating adsorption. Notably, rSPG contains partially hydrophobic amino acid residues, which could enhance interactions with other hydrophobic amino acid residues (such as ILE-253, MET-252, etc.) in IgG. on the fragment of IgG Fc, resulting in the special adsorption. Additionally, the rich O–H groups in the amino acid residues of rSPG could form hydrogen bonds with the COO- groups on the glycosylated residues in the Fc region of IgG, which served one of driving forces for IgG adsorption. Under acidic conditions, the solution contains higher concentration of acidic protons (H^+), causing the acidic groups to be protonated and weakening the strength of hydrogen bonds, thus resulting in reduced adsorption efficiency. Surface charge analysis indicates that the rSPG@Ni-MOF-74 composite exhibited a negative charge between pH 4 and 11, as shown in Fig. S4. Experimental results

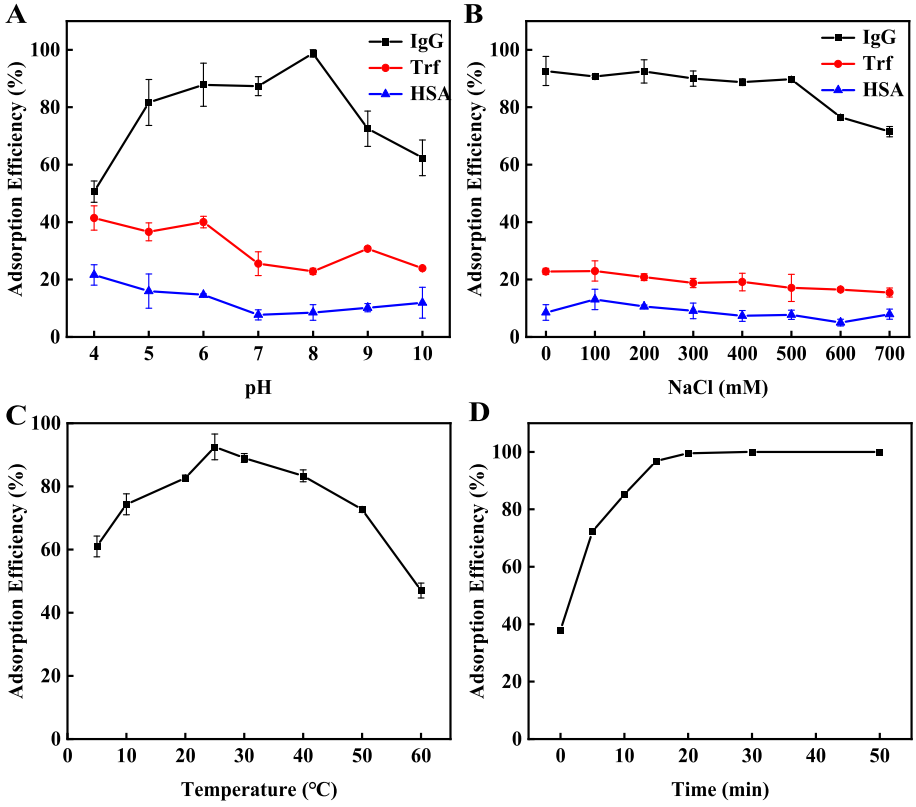

Fig. 2. PH-dependent adsorption behaviors of IgG, Trf and HSA onto rSPG@Ni-MOF-74 surface (A). Effect of the ionic strength of the adsorption efficiency of IgG, Trf and HSA (B). Effect of the adsorption temperature (C) and time (D) on adsorption efficiency of IgG. Protein solution: 100 μg mL^{-1}, 200 μL; rSPG@Ni-MOF-74: 0.1 mg.

displayed that the presence of a positive charge on the protein have not lead to favorable adsorption, indicating that electrostatic interactions are not the primary driving factor for protein adsorption onto the surface of rSPG@Ni-MOF-74. Additionally, the highest adsorption efficiency of HSA and Trf occurred in proximity to their individual isoelectric points. This proximity was due to the negative charge present on the protein surface when the pH surpasses their isoelectric points. Additionally, the negative charges on the surface of rSPG@Ni-MOF-74 lead to electrostatic repulsion between the negative charges on the protein surface and the material. This repulsive force become more pronounced with increasing pH levels, ultimately resulting in a reduction in adsorption efficiency. Due to the advantageous binding of IgG at pH 8.0 while exhibiting extremely low adsorption efficiency towards HSA and Trf, pH 8.0 was chosen as the selective separation condition for IgG. Compared to raw Ni-MOF-74 (Fig. S5), the rSPG@Ni-MOF-74 demonstrated significantly enhanced adsorption efficiency for IgG and reduced adsorption for two other proteins. The adsorption capacity of unmodified Ni-MOF-74 was primarily determined by its physicochemical properties, including surface charge, pore size, and various non-specific adsorption interactions, resulting in irregular and non-selective adsorption efficiency. In contrast, the modified rSPG selectively bonded to the Fc region of IgG molecules while preserving the functionality of their Fab regions, thus conferring good selectivity for IgG to rSPG@Ni-MOF-74.

In practical application, it is essential to take into consideration the influence of ionic strength because the desired protein species frequently exists alongside intricate matrices. As shown in Fig. 2B, it could be observed that the adsorption efficiency of rSPG@Ni-MOF-74 for IgG remained relatively stable or exhibits slightly increased within the salt concentration range spanning from 0 to 500 mmol L^{-1}, and decreased slowly at high ion concentrations (>500 mM). This suggested that low ion concentrations may promote the adsorption of IgG on rSPG@Ni-MOF-74, while high ion concentrations inhibit the adsorption effect. In contrast to IgG, the efficiency of HSA and Trf adsorption exhibited a slight increase followed by a decrease as the salt concentration increased. The initial increased was due to the revelation of hydrophobic domains of the protein induced by the concentration of salt ions under pH 8 conditions, augmenting the hydrophobic properties of the protein and leading to relatively elevated rates of adsorption. However, with the continued increase in salt levels, the rivalry between salt ions and protein molecules heightened, leading to a reduction in adsorption efficiency. In spite of this effect, in the scope of NaCl concentrations from 0 to 500 mM, the composite still maintained an efficiency of IgG adsorption exceeding 88 %, indicating that the main factor propelling IgG adsorption is the synergistic effect between hydrophobic interactions and hydrogen bonding. To obtain the satisfactory adsorption for subsequent investigation, a BR buffer with a concentration of 0.04 mM and pH 8.0, supplemented with a concentration of salt of 500 mM, was chosen as optimized condition. Fig. 2C and D displayed the effect of temperature and time on the IgG adsorption, we could observe that the best adsorption occurred at a temperature of 25 °C, and the adsorption efficiency progressively increase with longer adsorption times, reaching the adsorption equilibrium at 20 min.

3.3. Adsorption kinetics and isotherms

The adsorption kinetics of IgG on the rSPG@Ni-MOF-74 was investigated. As displayed in Fig. 3A, the adsorption capacities exhibited rapid growth attributed to the plentiful adsorption sites on the rSPG@Ni-MOF-74, plateauing upon reaching equilibrium within 30 min. To further discuss the adsorption kinetics, PFO kinetic model (equation (3)) and PSO kinetic model (equation (4)) were employed to fit the experimental data (Fig. 3B and C). According to Table S2, the adsorption kinetics of rSPG@Ni-MOF-74 for IgG better adhered the

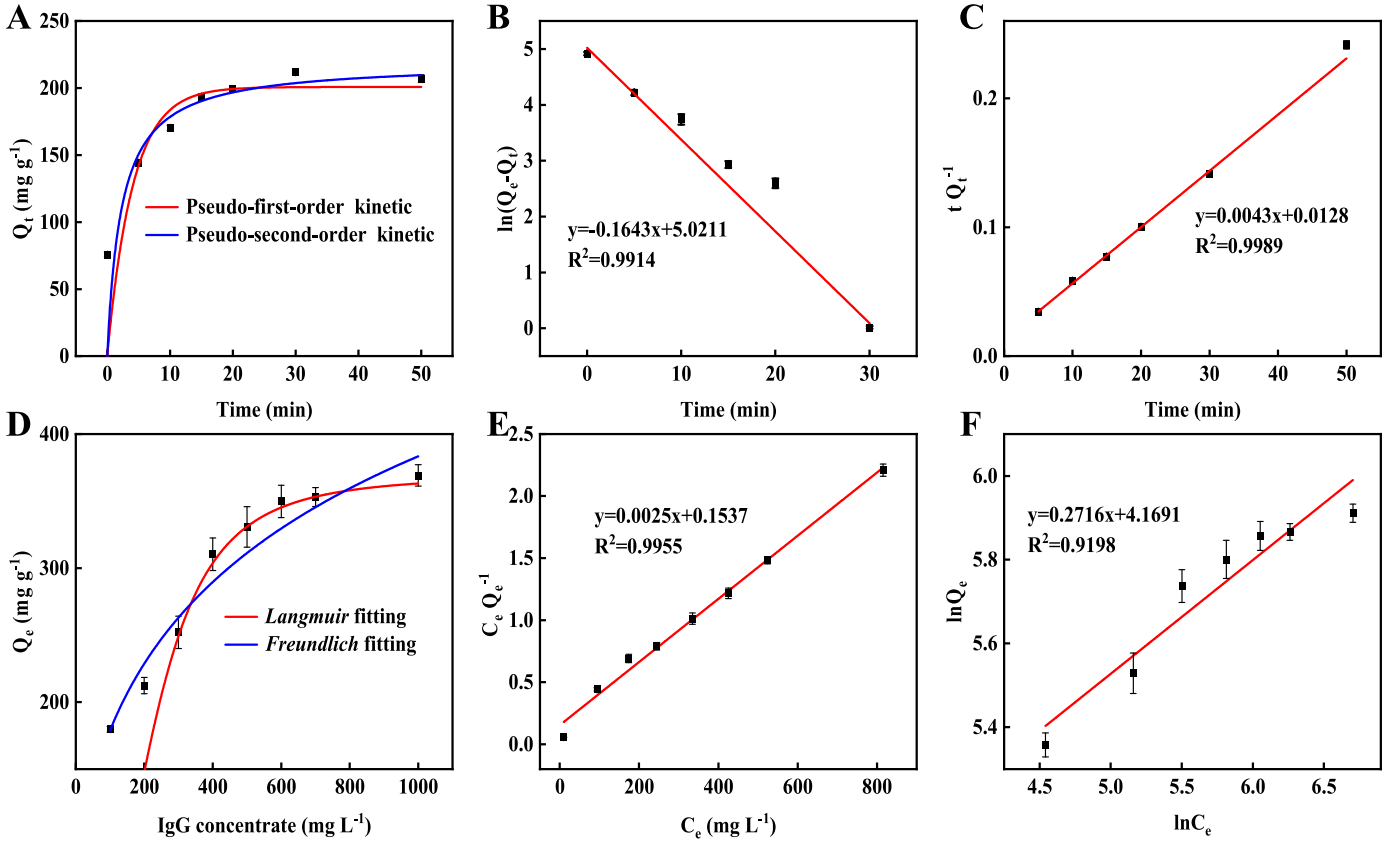

Fig. 3. (A) Effect of the contact time on IgG fitted by using pseudo-second-order (B) and pseudo-first-order (C) kinetic models. (D) Effect of IgG concentration on the adsorption and the corresponding nonlinear forms of *Langmuir* (E) and *Freundlich* (F) model for rSPG@Ni-MOF-74.

pseudo-second-order kinetic model ($R^2 = 0.9989$), indicating the presence of active sites capable of specifically recognizing IgG on rSPG@Ni-MOF-74. Fig. 3D depicted the dynamic adsorption isotherm of IgG onto the rSPG@Ni-MOF-74 composite at ambient temperature over a concentration scope of 100–1000 μg mL^{-1}. The adsorption model between rSPG@Ni-MOF-74 and IgG is further described using the *Langmuir* model (equation (5)) (Fig. 3E) and *Freundlich* model (equation (6)) (Fig. 3F), According to Table S3, the adsorption isotherm of IgG on rSPG@Ni-MOF-74 was better conformed to the *Langmuir* model ($R^2 = 0.9955$), indicating a monolayer adsorption behavior between rSPG@Ni-MOF-74 and IgG. In accordance with the *Langmuir* model, the maximum theoretical adsorption capacity amounts to 393.7 mg g^{-1}. Compared with other reported adsorbents, rSPG@Ni-MOF-74 exhibited a relatively higher adsorption capacity (Table 1). 3.4.The desorption of IgG from rSPG@Ni-MOF-74.

To perform subsequent biological studies in practical applications, appropriate stripping agents were used to separate IgG adsorbed on the surface of rSPG@Ni-MOF-74. Various potential stripping agents, including imidazole (0.1 mol L^{-1}), BR buffer (pH 5.0), Tris (0.1 mol L^{-1}), NaCl (3 mol L^{-1}), H_2O, and 0.5 % SDS solution, have been selected for the elution of IgG from rSPG@Ni-MOF-74. As shown in Fig. 4A, a recovery rate of 93.5 % was achieved by using 0.5 % SDS and other eluents showed limited recovery of IgG. Therefore, 0.5 % (m/m) SDS solution was used as the stripping agent to recover IgG adsorbed from rSPG@Ni-MOF-74 for subsequent studies. In addition, we also examined the reusability of rSPG@Ni-MOF-74, after consecutive cycles of adsorption and elution experiments, rSPG@Ni-MOF-74 could maintain its adsorption capacity for IgG. As depicted in Fig. 4B, the process of repeated IgG adsorption and elution experiment was conducted five times, resulting in a slight decrease in the efficiency of rSPG@Ni-MOF-74 for IgG adsorption. However, after five cycles, its adsorption efficiency remained above 60 %, indicating that the prepared rSPG@Ni-MOF-74 has good recyclability and stability as an adsorbent.

Circular dichroism (CD) spectroscopy was conducted to assess the alterations in the conformation of IgG. The negative peak observed in the water-soluble IgG standard appears at 218 nm, indicating the β-fold structure of IgG (Fig. S6a). However, the peak position of the IgG solution recovered after SDS elution has shifted, indicating some modifications to IgG throughout the experimental process (Fig. S6c). This alteration could be attributed to two potential factors. Firstly, the adsorption process between the composite of rSPG@Ni-MOF-74 and IgG could potentially lead to a conformational alteration. Secondly, the SDS eluent may also potentially lead to alterations in the conformation of IgG throughout the elution phase. Additional investigation was required to unveil the specific mechanisms behind the conformational alterations in IgG and to ascertain the influence of the composite material or eluent on its structure. We dissolved IgG in a solution containing 0.5 % SDS and conducted CD spectrum analysis to investigate the reason of the conformational alteration in IgG. The peak observed in the solution corresponded to that of the purified IgG, suggesting that SDS was probably accountable for the alteration (Fig. S6b). To ascertain the potential reversibility of the conformational change, SDS was removed from the IgG eluate via ultrafiltration using an ultrafiltration tube (10 kDa), followed by multiple rounds of ultrafiltration with water. However, the CD spectrum of the IgG post-ultrafiltration did not entirely align with that of the standard water-soluble IgG, indicating that the structural modifications caused by SDS were permanent (Fig. S6d). The result could be explained by the fact that IgG undergoes aggregation after SDS elution, rendering it challenging to return its initial conformation. These aggregates stem from increased interactions between proteins and non-specific attractive forces. Nonetheless, protein clustering can alter the secondary structure, leading to alterations in the CD spectrum. To prevent aggregation and maintain the protein in its monomeric state, protectants or stabilizing agents can be added in the following steps.

Table 1
The comparison of adsorption capacities for IgG with other adsorbents.

Absorbents	Adsorption capacity (mg g^{-1})	Equilibrium time (min)	Ref
UiO@GO@PEG	139.6	30	[29]
Co-MOF-OH	97.7	30	[30]
PAAm-Alg-ECH-P-Tyr	91.8	120	[31]
Fe_3O_4@PEI@POM1 NPs	304.4	10	[32]
MIL-125(Ti)	232.6	30	[33]
rSPG@Ni-MOF-74	393.7	20	This work

3.4. IgG isolation from human whole blood by the rSPG@Ni-MOF-74

The practical utility of rSPG@Ni-MOF-74 in selectively adsorb IgG was illustrated by isolating IgG from human whole blood. The serum samples were diluted 200-fold with buffer solution containing 500 mM NaCl (pH 8.0), and then experience adsorption/desorption process as described in the experimental section. The adsorbed IgG was recovered using a SDS(0.5 % w/w) solution. Subsequently, SDS-PAGE experiments were conducted using voltages of 80 mV and 120 mV. The protein bands were stained with 0.1 % (w/v) Coomassie Brilliant Blue R-250 and destained with a 250 mM KCl solution. As results in Fig. 5, numerous protein bands were clearly observed in the human serum sample (Lane 2), spanning a range from 20 to 200 kDa, primarily corresponding to HSA (66.4 kDa), Trf (79 kDa), IgG Heavy Chain (50 kDa), and IgG Light Chain (25 kDa). Only two prominent protein bands are seen in the eluent (Lane 5), corresponding to the positions of the standard IgG heavy chain and IgG light chain (Lane 6). In addition, the serum treated with rSPG@Ni-MOF-74 (line 3) shows a significantly lower content of IgG compared with the serum before treatment with rSPG@Ni-MOF-74 (line 2), indicating successful separation of IgG from the human serum by rSPG@Ni-MOF-74. These clearly demonstrated the excellent potential of rSPG@Ni-MOF-74 for the selective enrichment and separation of IgG from real samples coexisting with other proteins.

To further validate the efficiency of the rSPG@Ni-MOF-74 composite in purifying IgG and its potential utility in proteomics, serum samples were subjected to LC-MS/MS analysis before and after adsorption, as well as the IgG elute from the rSPG@Ni-MOF-74. The objective was to evaluate the specificity and selectivity of rSPG@Ni-MOF-74 during the separation and purification of IgG, and to investigate whether there are any alterations in the protein composition throughout the entire process. The IgG content in serum significantly decreased after adsorption by rSPG@Ni-MOF-74 (Fig. 6B). Furthermore, the content of IgG in the eluent reached 55.3 % (Fig. 6C), which was the highest proportion, demonstrating the effective enrichment of IgG by rSPG@Ni-MOF-74.

4. Conclusion

In this study, we develop a novel solid-phase extraction agent, rSPG@Ni-MOF-74, by modifying Ni-MOF-74 with rSPG (His-tag), and applied it for the separation and enrichment of IgG from human serum. The presence of His-tag in rSPG allows for the formation of a metal coordination bond with unsaturated Ni^{2+} sites, as each histidine residue carries an imidazole group. This enables rSPG to firmly bind to the surface of Ni-MOF-74. The successful synthesis of rSPG@Ni-MOF-74 was confirmed through analytical methods including SEM, FT-IR, XRD, XPS, TEM, and BET. The synthesized rSPG@Ni-MOF-74 exhibites high adsorption selectivity towards IgG through synergy of multiple forces, with a high theoretical adsorptive capacity of 393.7 mg g^{-1}. Further confirmation of the selective separation of IgG from actual biological samples was obtained through SDS-PAGE analysis. Meanwhile, LC-MS/MS analysis of serum samples validated the effectiveness of rSPG@Ni-MOF-74 in separating IgG. This underscores the potential of the work in broadening the scope of proteins identified and highlights the

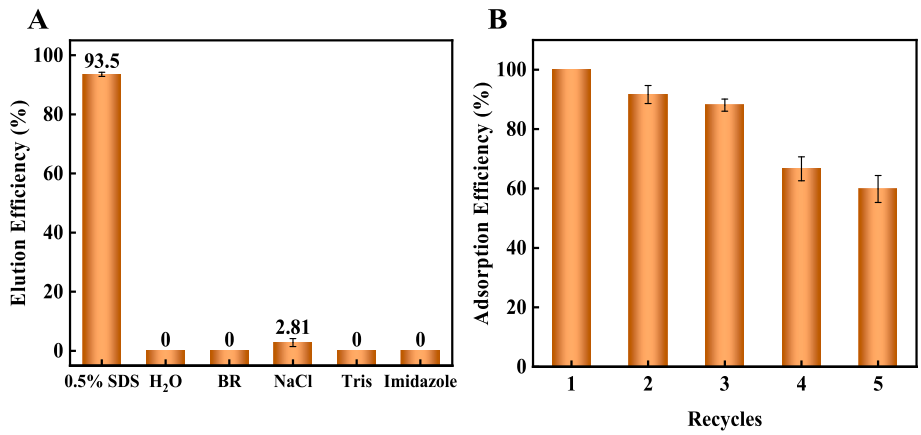

Fig. 4. (A) The elution efficiency of the adsorbed IgG from rSPG@Ni-MOF-74 by using various eluents. (B) The adsorption performance rSPG@Ni-MOF-74 after the continuous five adsorption/desorption cycles of IgG (100 μg mL^{-1}).

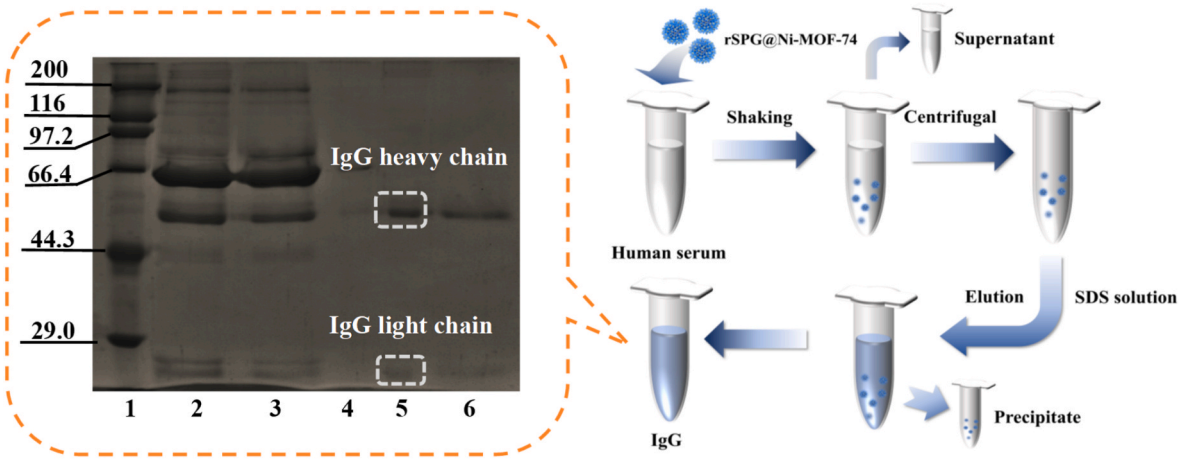

Fig. 5. Isolation of immunoglobulin G from human serum by rSPG@Ni-MOF-74. SDS-PAGE assay results. Lane 1: molecular weight standard (kDa); Lane 2: 200-fold diluted human serum without other pretreatment; Lane 3: 200-fold diluted human serum after adsorption by rSPG@Ni-MOF-74 nanoparticles; Lane 4: the supernatant obtained after washing the IgG-adsorbed rSPG@Ni-MOF-74 nanoparticles with 0.1 mol L^{-1} imidazole; Lane 5: recovered solution from rSPG@Ni-MOF-74 nanoparticles; Lane 6: IgG standard of 100 μg mL^{-1}.

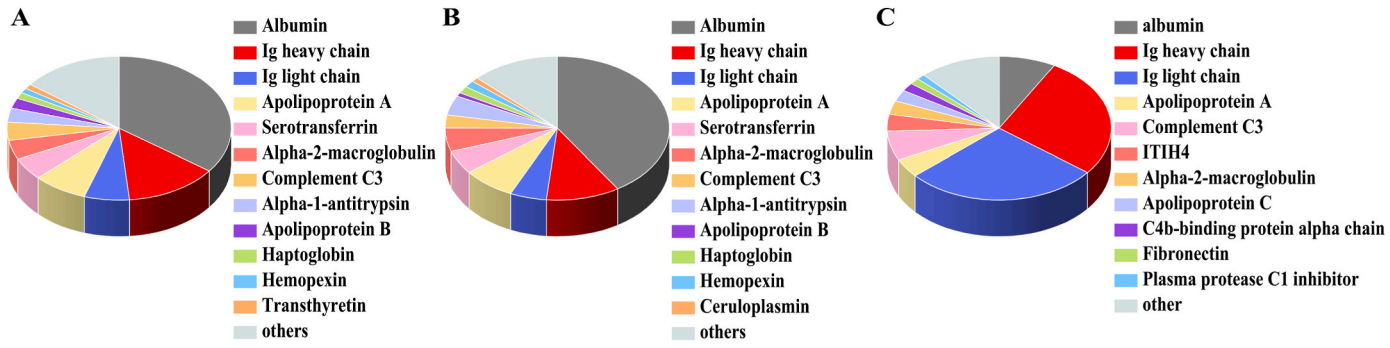

Fig. 6. Mass spectrometry data. Distribution of the top 12 most abundant proteins in serum (A), the supernatant after isolation of IgG with rSPG@Ni-MOF-74 composite (B) and the recovered solution after SDS removal (C).

significance of the rSPG@Ni-MOF-74 in proteomic analysis.

CRediT authorship contribution statement

Kai Wang: Writing – review & editing, Validation, Funding acquisition. **Hongjin Zhang:** Writing – review & editing, Software, Investigation. **Nishan Jin:** Supervision, Investigation. **Yutian Zhou:** Investigation. **Xinli Guo:** Investigation. **Wenbin Zhong:** Investigation. **Xin Li:** Investigation, Funding acquisition. **Xuwen Li:** Writing – review & editing, Investigation. **Yang Zhang:** Writing – original draft, Project administration, Methodology, Investigation, Funding acquisition, Conceptualization.

Declaration of competing interest

The authors declare that they have no known competing financial interests or personal relationships that could have appeared to influence the work reported in this paper.

Data availability

No data was used for the research described in the article.

Acknowledgments

The authors appreciate financial supports from the Shenyang Science and Technology Talent Special Project (RC230022), Natural Science Foundation of Liaoning Province (2023-MSLH-288), Science Research Foundation of Education Department for Liaoning Province (LJKMZ20221790), and Science Research Foundation of Education Department for Liaoning Province (2023JH2/101300079).

Appendix B. Supplementary data

Supplementary data to this article can be found online at https://doi.org/10.1016/j.talanta.2024.126535.

References

[1] R. Djurup, Immunochemical quantitation of IgG subclass proteins and IgG subclass antibodies: status and perspectives, Monogr. Allergy 23 (1988) 12–17.
[2] H.W. Schroeder, L. Cavacini, Structure and function of immunoglobulins, Allergy Clin Immunol 125 (2010) S41–S52.
[3] W. Zhou, M. Graner, C. Beseler, T. Domashevich, S. Selva, G. Webster, A. Ledreux, Z. Zizzo, M. Lundt, E. Alvarez, X. Yu, Plasma IgG aggregates as biomarkers for multiple sclerosis, Clin. Immunol 256 (2023) 109801.
[4] S. Özen Bölük, N. Gülez, C. Karkıner, Ö. Soyöz, F. Çelebi Çelik, M.Ş. Kaya, I. Akay Hacı, I. Taşkırdı, Ö. Akçal, F. Genel, The effect of subcutaneous immunoglobulin replacement therapy on serum IgG levels in patients with primary immunodeficiency, Trends Pediatr. 4 (2023) 103–108.
[5] R. Goto, R. Inuzuka, T. Shindo, Y. Namai, Y. Oda, Y. Harita, A. Oka, Relationship between post-IVIG IgG levels and clinical outcomes in Kawasaki disease patients: new insight into the mechanism of action of IVIG, Clin. Rheumatol. 39 (2020) 3747–3755.
[6] G.R. Ma, R.Q. Xu, W. Pei, Y. Zhang, R. Ma, R. Yang, Z. Zhao, Y. Li, C.J. Feng, D. Jin, W. Ma, Y.M. Ma, Z.R. Ma, Screening and validation of an alkaline-tolerant biomimetic affinity chromatography A5-87 resin for purification of discarded bovine serum Immunoglobulin G, J. Chromatogr A 1714 (2024) 464580.
[7] L. Wang, H.K. Trang, J. Desai, Z.D. Dunn, D.D. Richardson, R.K. Marcus, Fiber-based HIC capture loop for coupling of protein A and size exclusion chromatography in a two-dimensional separation of monoclonal antibodies, Anal. Chim. Acta 1098 (2020) 190–200.
[8] B. Radovani, G. Lauc, I. Gudelj, Storage stability and HILIC-UHPLC-FLR analysis of immunoglobulin G N-glycome from saliva, Anal. Bioanal. Chem. 415 (2023) 6985–6993.
[9] E.L. Rodriguez, S. Poddar, S. Iftekhar, K. Suh, A.G. Woolfork, S. Ovbude, A. Pekarek, M. Walters, S. Lott, D.S. Hage, Affinity chromatography: a review of trends and developments over the past 50 years, J. Chromatogr B 1157 (2020) 122332.
[10] J. Engelke, J. Brandt, C. Barner-Kowollik, A. Lederer, Strengths and limitations of size exclusion chromatography for investigating single chain folding-current status and future perspectives, Polym. Chem. 10 (2019) 3410–3425.
[11] D. Taylor, B. Sousa, G. West, A. Neo Huipeng, A.F. Lopez Clavijo, Methods for the relative quantitation of human plasma lipidome using liquid chromatography coupled with mass spectrometry using minimal sample manipulation, Rapid Commun. Mass Spectrom. 38 (2024) e9641.
[12] F.F. Magalhães, M.R. Almeida, S.F. Soares, T. Trindade, M.G. Freire, A.L. Daniel-da-Silva, A.P.M. Tavares, Recovery of immunoglobulin G from rabbit serum using κ-carrageenan-modified hybrid magnetic nanoparticles, Int. J. Biol. Macromol. 150 (2020) 914–921.
[13] X.M. Wang, Z.J. Hu, P.F. Guo, M.L. Chen, J.H. Wang, Boron-modified defect-rich molybdenum disulfide nanosheets: reducing nonspecific adsorption and promoting a high capacity for isolation of Immunoglobulin G, ACS Appl Mater 12 (2020) 43273–43280.
[14] J. Yang, Y. Yang, Metal-organic frameworks for biomedical applications, Small 16 (2020) 1906846.
[15] Z.J. Hu, X.M. Wang, X.W. Chen, Bisphosphorylated fructose-modified magnetic Zr-Organic framework: a dual-hydrophilic sorbent for selective adsorption of immunoglobulin G, Anal. Chim. Acta 1112 (2020) 16–23.
[16] C.L. Li, J. Shen, K.B. Wu, N.J. Yang, Metal centers and organic ligands determine electrochemistry of metal-organic frameworks, Small 18 (2022) 2106607.
[17] Y.Y. Zhang, W. Xu, J.F. Cao, Y. Shu, J.H. Wang, Ionic liquid modification of metal-organic framework endows high selectivity for phosphoproteins adsorption, Anal. Chim. Acta 1147 (2021) 144–154.
[18] C.R. Goward, J.P. Murphy, T. Atkinson, D.A. Barstow, Expression and purification of a truncated recombinant streptococcal protein G, Biochem. J. 267 (1990) 171–177.
[19] S.G. Kim, J. Kim, M.Y. Kim, J.M. Park, J. Jose, M. Park, Autodisplay of streptococcal protein G for construction of an orientation-controlled immunoaffinity layer, Analyst 148 (2023) 742–751.
[20] Y. Zhou, S. Yuan, Q. Liu, D. Yan, Y. Wang, L. Gao, J. Han, H. Shi, Synchronized purification and immobilization of his-tagged β-glucosidase via Fe_3O_4/PMG core/shell magnetic nanoparticles, Sci. Rep. 7 (2017) 41741.
[21] L. Lei, Y. Cheng, C. Chen, M. Kosari, Z. Jiang, C. He, Taming structure and modulating carbon dioxide (CO_2) adsorption isosteric heat of nickel-based metal organic framework (MOF-74(Ni)) for remarkable CO_2 capture, J. Colloid Interface Sci. 612 (2022) 132–145.
[22] Y. Yu, W. Li, H. Yang, Q. Wei, L. Hou, Z. Wu, Y. Jiang, C. Lv, Y. Huang, J. Tang, 4-Methyl-5-vinyl thiazole modified Ni-MOF/g-C_3N_4/CdS composites for efficient photocatalytic hydrogen evolution without precious metal cocatalysts, J. Colloid Interface Sci. 651 (2023) 221–234.
[23] Y. Xiao, W. Wei, M.J. Zhang, S. Jiao, Y.C. Shi, S.J. Ding, Facile surface properties engineering of high-quality graphene: toward advanced Ni-MOF heterostructures for high-performance supercapacitor electrode, ACS Appl. Energy Mater. 2 (2019) 2169–2177.
[24] X.H. Niu, S.M. Yan, L.T. Wang, J.L. Chen, R. Zhao, H.X. Li, J. Liu, K.J. Wang, Induction of chiral polymers from metal-organic framework for stereoselective recognition, Anal. Chim. Acta 1196 (2022) 339546.
[25] K. Tian, Y.S. Ma, Y.K. Liu, M.H. Wang, C.P. Guo, L.H. He, Y.P. Song, Z.H. Zhang, M. Du, Hierarchically structured hollow bimetallic ZnNi MOF microspheres as a sensing platform for adenosine detection, Sensor Actuat B-chem 303 (2020) 127199.
[26] C.H. Li, W.X. Yang, X.S. Zhang, Y. Han, W.Z. Tang, T.L. Yue, Z.H. Li, A 3D hierarchical dual-metal organic framework heterostructure up-regulating the pre-concentration effect for ultrasensitive fluorescence detection of tetracycline antibiotics, J. Mater. Chem. C 8 (2020) 2054–2064.
[27] Q.Y. Zhang, Q.Z. Luo, Y.P. Wu, R.F. Yu, J.S. Cheng, Y.T. Zhang, Construction of a Keggin heteropolyacid/Ni-MOF catalyst for esterification of fatty acids, RSC Adv. 11 (2021) 33416–33424.
[28] L. Reguera, Y. Avila, E. Reguera, Transition metal nitroprussides: crystal and electronic structure, and related properties, Coord. Chem. Rev. 434 (2021) 213764.
[29] Z.J. Hu, X.M. Wang, J.H. Wang, X.W. Chen, PEGylation of metal-organic framework for selective isolation of glycoprotein immunoglobulin G, Talanta 208 (2020) 120433.
[30] Z.J. Hu, J. Meng, X.M. Wang, W.T. Li, X.W. Chen, Tailoring the surface properties of Co-based metal-organic frameworks for highly efficient and selective enrichment of Immunoglobulin G, ACS Appl. Mater. Interfaces 12 (2020) 55453–55459.
[31] C. Marcuz, C. Alves Mourão, K. Haupt, S.M. Alves Bueno, Performance of phospho-L-tyrosine immobilized onto alginate/polyacrylamide-based cryogels: effect of ligand coupling on human IgG adsorption and Fab fragments separation, J. Chromatogr. B 1165 (2021) 122530. J. Chromatogr B 1165 (2021) 122530.
[32] D.D. Zhang, Z.Y. Guo, P.F. Guo, X. Hu, X.W. Chen, J.H. Wang, Polyoxometalate-coated magnetic nanospheres for highly selective isolation of Immunoglobulin G, ACS Appl. Mater. Interfaces 10 (2018) 21876–21882.
[33] Z.X. Chi, X. Wu, Q.Q. Zhang, F.Y. Zhai, Z.S. Xu, D.D. Zhang, Q. Chen, Titanium-based metal-organic framework MIL-125(Ti) for the highly selective isolation and purification of immunoglobulin G from human serum, J. Separ. Sci. 45 (2022) 3754–3762.